# Fano stability diagram of a symmetric triple quantum dot

Michael Niklas, Andreas Trottmann, Andrea Donarini, and Milena Grifoni*

*Institute for Theoretical Physics, University of Regensburg, 93040 Regensburg, Germany*

(Dated: October 27, 2016)

The Fano factor stability diagram of a $C_{3v}$ symmetric triangular quantum dot is analysed for increasing electron fillings $N$. At low filling, conventional Poissonian and sub-Poissonian behavior, caused by the interplay of electron-electron interactions and Fermi statistics, is found. At larger filling, $N \geq 2$, super-Poissonian noise and a peculiar bias voltage dependence of the Fano factor are observed at Coulomb and interference blockade. An analysis of the Fano map unravels a nontrivial electron bunching mechanism arising from the presence of degenerate many-body states combined with orbital interference and Coulomb interactions.

Current fluctuations in out of equilibrium nanoscale systems can yield information about relevant transport mechanisms not accessible from the knowledge of the average current only [1]. While sub-Poissonian noise is ubiquitous in fermionic tunneling structures, fermionic bunching leading to enhanced shot noise is a signature of subtle quantum correlations. For example, in single level quantum dot systems, the interplay between Pauli principle and repulsive Coulomb interactions yields Poissonian shot noise (corresponding to a Fano factor $F = 1$, see Fig. 1(a)), and sub-Poissonian noise with $1/2 < F < 1$ in the Coulomb blockade and sequential transport regimes, respectively [2–7]. The sub-Poissonian Fano factor naturally originates from the requirement of charge conservation at zero frequency and the fact that each tunneling barrier can be regarded as an independent source of Poissonian noise [8]. The enhancement of the shot noise requires a multilevel structure of the quantum dot [4, 8, 9] or complex multiple quantum dot devices [11–14]. Independent of the details of the nanosystems, super-Poissonian noise implies the presence of slow and fast channels, and mechanisms which, virtually (cotunneling) or really (sequential tunneling), occasionally allow for charge transfer on a time scale much shorter than the average residence time in the slow channel state. The mechanism of dynamical channel blockade [4, 9], giving rise to super-Poissonian noise, is illustrated in Fig. 1(b).

In this letter we investigate the Fano stability diagram of a $C_{3v}$ symmetric triangular triple quantum dot (TQD), schematically sketched in Fig. 1(d), as a function of its occupation. TQDs are the smallest systems where the interplay of statistics, Coulomb interactions and geometry allows one the study of peculiar many-body effects such as super-exchange induced triplet-singlet transition [2], many-body interference [1, 5, 13], cellular automata phenomena [18], charge frustration [19–21], or channel blockade [22]. TQDs have been recently realized in lateral semiconducting heterostrucures [18, 19, 22, 23], which are tunable down to the few electron regime by means of plunger and depletion gates [23], and by means of atomic STM manipulation [24]. In the latter experiment, orbital
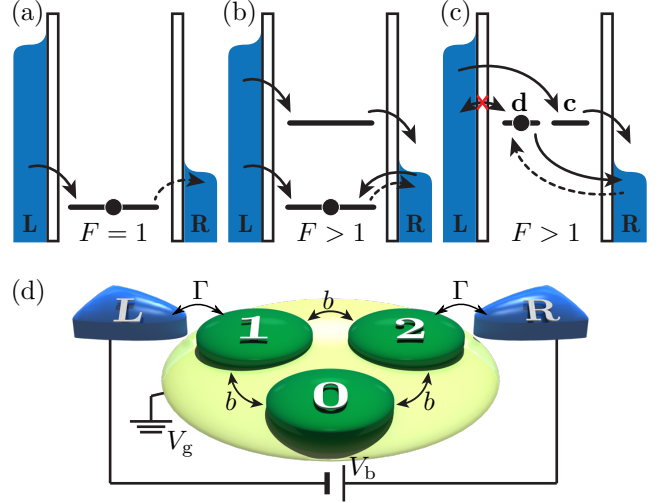


FIG. 1. (a) Single level quantum dot in the Coulomb blockade regime with Fano factor $F = 1$. (b) If an excited state is present in the bias window of a Coulomb blockaded quantum dot, electron bunching through the excited state yields super-Possonian noise ($F > 1$). (c) Interference of energy degenerate orbitals gives rise to coupled, $c$, and decoupled, $d$, states, and in turn to super-Poissonian noise. Solid arrows show fast processes, dashed ones the dominant slow processes. (d) A gated triangular triple quantum dot (TQD) features all the three dynamical situation sketched in (a)-(c) depending on the occupation number and on the applied bias and gate voltages $V_b$ and $V_g$, respectively.

degeneracy in a $C_{3v}$ symmetric triangular dot could be demonstrated.

So far, investigations of transport noise have been restricted to set-ups in which the $C_{3v}$ symmetry of an isolated TQD is broken in various ways, e.g. by assuming unequal interdot hoppings and/or onsite energies [12, 13, 25–27]. These asymmetries remove orbital degeneracies and hence the possibility to observe current suppression due to the destructive interference of energy degenerate states [28]. In this work we demonstrate that the Fano map of a $C_{3v}$ symmetric, weakly coupled TQD is characterized by regions of super-Poissonian noise *out-*

*side* the Coulomb blockade region, see Fig. 1(c), with specific fractional values of the Fano factor being a signature of such many-body interference. Inside the Coulomb blockade region, large super-Poissonian Fano factors due to an interplay of dynamical channel blockade [4, 9] and interference are identified.

*Model and method.* – We examine a single-electron transistor model described by the total Hamiltonian $H = H_{\text{TQD}} + H_{\text{tun}} + H_{\text{res}}$. The TQD spectrum derives from a three-site Hubbard model with hopping $b < 0$, onsite Coulomb repulsion $U$ and extended by the inter-site repulsion $V$, which is adequate for many TQDs [3]. The according Hamiltonian is

$$H_{\text{TQD}} = \xi \sum_{i\sigma} n_{i\sigma} + b \sum_{i\neq j,\sigma} d^{\dagger}_{j\sigma} d_{i\sigma}$$
$$+ U \sum_i \left(n_{i\uparrow} - \frac{1}{2}\right)\left(n_{i\downarrow} - \frac{1}{2}\right) \quad (1)$$
$$+ V \sum_{i<j} \left(n_{i\uparrow} + n_{i\downarrow} - 1\right)\left(n_{j\uparrow} + n_{j\downarrow} - 1\right),$$

where $\xi = \varepsilon - e\alpha V_{\text{g}}$ includes the onsite energy $\varepsilon$ and the effects of an applied gate voltage $V_{\text{g}}$ with level arm $\alpha$. Here, operators $d^{\dagger}_{i\sigma}$ and $d_{i\sigma}$ create and annihilate an electron with spin projection $\sigma$ in dot $i = 0, 1, 2$, and $n_{i\sigma} = d^{\dagger}_{i\sigma} d_{i\sigma}$, cf. Fig. 1(d). Due to the $C_{3v}$ symmetry, such Hamiltonian is invariant under rotations of $2\pi/3$ around an axis passing through the center of the TQD. Moreover, $H_{\text{TQD}}$ also conserves particles and spin. Using these symmetries, we have been able to calculate the whole energy spectrum and the eigenvectors $|N, E; S, S_z, L_z\rangle$ of $H_{\text{TQD}}$ in analytic form (see Supplementary Material, Tables I and II). The quantum numbers refer to the eigenvalues of the occupation number operator $N$, the energy $E$, the eigenvalues of the spin operators $S^2$ and $S_z$, and of the component along the rotation axis, $L_z$, of the total angular momentum. The two leads are considered as reservoirs of non-interacting electrons at chemical potentials $\mu_{L/R} = \mu_0 \pm eV_{\text{b}}/2$ for the left ($L$) and right ($R$) lead, with $V_{\text{b}}$ the applied bias voltage. The corresponding Hamiltonian is $H_{\text{res}} = \sum_{\alpha k\sigma} \xi_{\alpha k} c^{\dagger}_{\alpha k\sigma} c_{\alpha k\sigma}$, with $\alpha = L, R$. Finally, tunneling between TQD and leads is described by $H_{\text{tun}} = \sum_{\alpha k\sigma} \sum_i \left(t^*_{\alpha i} c^{\dagger}_{\alpha k\sigma} d_{i\sigma} + t_{\alpha i} d^{\dagger}_{i\sigma} c_{\alpha k\sigma}\right)$. In the following, we consider equal coupling to the left and right leads, and set the coupling constants $t_{L1} = t_{R2} = t$ and otherwise $t_{\alpha i} = 0$. We identify for later convenience $d_{1\sigma} = d_{L\sigma}$, $d_{2\sigma} = d_{R\sigma}$.

To compute the current and shot noise we use a master equation approach for the generalized reduced density matrix $\rho_\chi = \text{Tr}_{\text{res}} \{e^{i\chi N_{\text{R}}}\rho\}$, where $\chi$ and $N_R$ are the counting field and number operator for the right lead, and $\rho$ the total density operator [6, 30]. A truncation to second order in $H_{\text{tun}}$ yields the generalized master equation $\dot{\rho}_\chi = \left[\mathcal{L} + (e^{i\chi} - 1)\mathcal{J}^+ + (e^{-i\chi} - 1)\mathcal{J}^-\right]\rho_\chi$
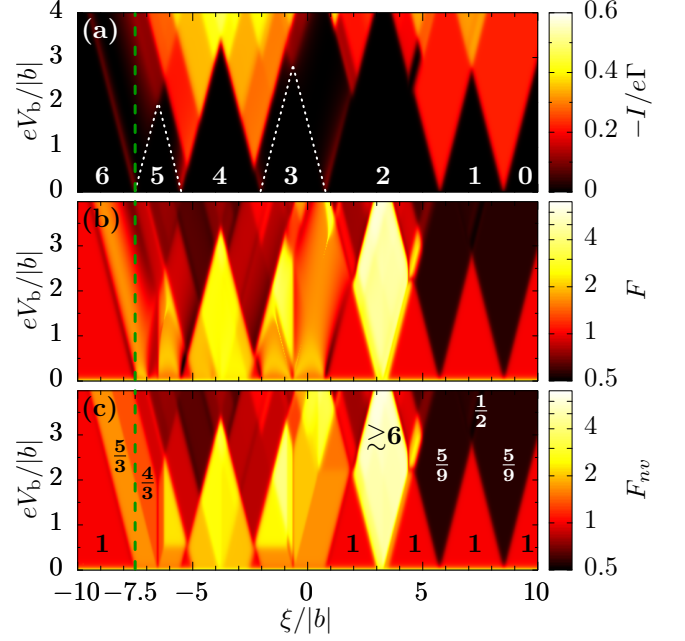


FIG. 2. Current and Fano factors vs applied gate and bias voltages. (a) Average current where the number of electrons in the blockade regions is displayed. The white dotted lines delimit regions where transport is inhibited due to Coulomb blockade. (b) Fano factor and (c) Fano factor without Lamb shifts due to virtual transitions. Some values discussed in the text are indicated. Parameters used for the simulations are $U = 5|b|$, $V = 2|b|$, $k_{\text{B}}T = 0.002|b|$, $\Gamma = |b|$ and $b = -1$.

[31], where $\mathcal{L}$ is the Liouville superoperator, and we defined the current superoperators for increasing, $\mathcal{J}^+$, and decreasing, $\mathcal{J}^-$, the number of electrons in the right lead. This results in the equations for the stationary reduced density matrix, $\rho^\infty = \lim_{t\to\infty} \rho_{\chi=0}$, and the moments $\mathcal{F}^\infty_k = \lim_{t\to\infty} d^k/d(i\chi)^k \rho_\chi|_{\chi=0}$. Introducing the traceless part of the first moment, $\mathcal{F}^\infty_{1\perp} = (1 - \rho^\infty \text{Tr}_{\text{TQD}})\mathcal{F}^\infty_1$, one finds in particular

$$\mathcal{L}\rho^\infty = -\frac{i}{\hbar}[H_{\text{TQD}} + H_{\text{LS}}, \rho^\infty] + \mathcal{L}_t \rho^\infty = 0,$$
$$\mathcal{L}\mathcal{F}^\infty_{1\perp} = \left(I - \mathcal{J}^+ + \mathcal{J}^-\right)\rho^\infty, \quad (2)$$

where $H_{\text{LS}}$ is an effective Hamiltonian accounting for Lamb shifts due to virtual excitations [5, 32], and $\mathcal{L}_t$ is the tunneling part of the Liouvillian. Importantly, the operatorial form of Eq. (2) allows us to fully account for interference effects captured in the off-diagonal elements of $\rho^\infty$. The current $I$ (first cumulant) and shot noise $S$ (second cumulant) in turn follow as [31]

$$I = -e\, \text{Tr}_{\text{TQD}} \left(\mathcal{J}^+ - \mathcal{J}^-\right)\rho^\infty, \quad (3)$$
$$S = e^2 \text{Tr}_{\text{TQD}} \left[2\left(\mathcal{J}^+ - \mathcal{J}^-\right)\mathcal{F}^\infty_{1\perp} + \left(\mathcal{J}^+ + \mathcal{J}^-\right)\rho^\infty\right].$$

As a dimensionless measure for the relative noise strength we employ the Fano factor $F = S/e|I|$.

*Current and Fano maps.* – The stationary current is shown as a function of bias and gate voltage in Fig. 2(a). For comparison, the same parameters as in Ref. [28] were used. Notice that the closed topology of the TQD breaks the particle-hole symmetry otherwise present in linear triple dots [2]. The stability diagram displays Coulomb diamonds inside which current is exponentially suppressed (in second order in $H_{\mathrm{tun}}$) due to Coulomb blockade, but also regions outside the Coulomb diamonds with suppression due to orbital interference [5]. We have indicated with dotted lines the Coulomb diamonds when no longer visible due to the additional interference blockade. A measurement of the current alone, however, does not enable one to tackle down the different blockade mechanisms. This is in contrast to the Fano map, shown in Fig. 2(b), which displays a much richer structure than the current. In Fig. 2(c) we also show the Fano factor $F_{nv}$, which is obtained by neglecting the Lamb shift term $H_{\mathrm{LS}}$ in the stationary Eq. (2). Clearly, the virtual transitions responsible for the Lamb shifts *blur* the otherwise poligonal Fano pattern.

At first glance one can observe a sub-Poissonian shot noise $1/2 < F < 1$ in the transport regime and both Poissonian, $F = 1$, and super-Poissonian, $F > 1$, shot noise in the regions of vanishing current. Furthermore, $F$ diverges when $V_{\mathrm{b}} \to 0$ due to Johnson-Nyquist noise. Finally, vertical steps in the Fano factor are clearly visible at the center of the 3- and 5-particles Coulomb diamonds. At these positions the energy levels of the states with one electron more and less than the participating Coulomb- or interference-blocked state are aligned, and a little change in the gate voltage favors one or the other side in transport, leading to a sudden change in the statistics that is unaffected by the bias voltage [33, 34].

The complexity of the Fano pattern increases with growing electron filling, so from right to left. The breaking of electron-hole symmetry is strikingly revealed in a Fano factor smaller (larger) than one, in the transport (blockade) regions involving the $N = 0 \, (6)$ and $N = 1 \, (5)$ groundstates. Moreover, large values of $F$ are observed for intermediate filling. The Fano map at low filling is easily understood by observing that the one-electron groundstates $\{|1, E_{1_0}; 1/2, \pm 1/2, 0\rangle\}$ are only spin degenerate. Then, in the region with zero and one electron occupation, the Fano map resembles the one of the single impurity Anderson model, with $F = 5/9$ and $F = 1/2$ in the transport regions, and $F = 1$ at Coulomb blockade [7]. As shown below, subtle correlations are responsible for the super-Poissonian noise at larger filling.

*Interplay of channel blockade and interference.* – High values of $F$ for a doubly occupied TQD have already been noticed in Ref. [13] and interpreted in terms of the dynamical channel blockade mechanism sketched in Fig. 1(b). This requires a Coulomb blockaded level, and excited states in the transport window which provide a fast transport channel. The larger the degeneracy of the

excited states, the larger is the Fano factor [4]. In the presence of interference, however, the multiplicity of the involved states alone cannot properly account for the observed values of $F$ or $F_{nv}$. As shown in the Supplement, at Coulomb blockade and $\mu_L > \mu_R$ the Fano factor $F_{nv}$ of a system of fast, $(f)$, and slow, $(s)$, channels can be expressed in terms of effective filling rates $\Gamma_\alpha^p = R_\alpha^p \Gamma_\alpha$ as

$$F_{nv}^{CB} = 1 + \frac{2\Gamma_L^f}{\Gamma_L^s + \Gamma_R^s}, \qquad (4)$$

where $\Gamma_\alpha = 2\pi |t|^2 D_\alpha / \hbar$ is the bare tunneling rate for lead $\alpha$, proportional to the density of states at the Fermi energy $D_\alpha$. In the following we assume identical leads, such that $\Gamma_L = \Gamma_R = \Gamma$, see Fig. 1(d). The coefficients $R_\alpha^p$ weight the fast and slow channels, and account for both spin degeneracies and orbital interference. For our symmetric TQD the 2-particles groundstate $|2, E_{2_0}; 0, 0, 0\rangle$ is non degenerate, while the first set of excited levels is given by the sextuplet $\{|2, E_{2_1}; 1, S_z, \pm 1\rangle, S_z = 0, \pm 1\}$, due to both orbital and spin degeneracy (see Tables of the Supplement). By applying the formula (4) naively assuming that $R_\alpha^p$ is just the channel multiplicity ($R_\alpha^s = 1$ and $R_\alpha^f = 6$), we would expect $F_{nv}^{CB} = 7$, which is bigger than the observed value $F_{nv} \approx 6$. This discrepancy arises because the orbitally degenerate excited states can undergo interference blockade, thus yielding non trivial weights $R_\alpha^p$. The latter do not have in general a simple analytical form, since the involved many-body states are the sum of many Slater determinants. A fully analytical treatment is possible in the parameter region involving the $N = 6$ groundstate $|6, E_6; 0, 0, 0\rangle := |6\rangle$ and the $N = 5$ groundstate quadruplet $\{|5, E_{5_0}; 1/2, \pm 1/2, \pm 1\rangle\}$. This situation is addressed below.

*Interference blockade at the $5_0 \leftrightarrow 6$ resonance.* – When a set of orbitally degenerate levels participate in transport, interference can yield a (many-body) state completely decoupled from one lead [28] such that electrons in the dot can only leave via thermal activation through the other lead or via virtual excitations, see Fig. 1(c). This yields current suppression. If this blocking channel is decoupled at the left lead, the Fano factor is

$$F_{nv}^{IB} = 1 + 2\frac{\Gamma_R^f}{\Gamma_R^s}, \qquad (5)$$

as shown in the Supplementary Material. Bias traces of currents and Fano factors at the gate voltage corresponding to $\xi = -7.5|b|$ (green line in Fig. 2) are shown in Fig. 3. The current $I_{nv}$, which does not account for the Lamb shifts, is exponentially suppressed in the voltage range $0.5 < eV_{\mathrm{b}}/|b| < 3.5$. The associated Fano factor takes the values $F_{nv} = 5/3$ at low bias, and $F_{nv} = 4/3$ above $eV_{\mathrm{b}}/|b| = 2$, when transitions from $5_0$ to the 4-particle groundstates $\{|4, E_{4_0}; 1, S_z, 0\rangle\}$ dominate the bottleneck process for transport [35]. Virtual transitions modify this

picture: the current $I$ (Fano factor $F$) varies with bias voltage and has a minimum (maximum) at $eV_b \approx |b|$.

For the blockade due to an orbital degenerate ground-state with one coupled and one decoupled state one would naively expect $R_R^f = R_R^s$ and therefore a Fano factor $F_{nv}^{IB} = 3$, as found in many systems [4, 9, 11, 12]. The values $F_{nv} = 5/3$ and $4/3$ again indicate that interference requires a more precise analysis.

To this extent, let us observe that since the total Hamiltonian $H$ conserves particles, energy and spin, the stationary density matrix $\rho^\infty$ has a block diagonal structure, with blocks $\rho^{NSS_z}(E)$ of definite $N$, $S$, $S_z$, and $E$ [36]. Due to the equivalence of the configurations with different $S_z$ for the dynamics, we introduce the matrices $\rho^N_{L_z L_z'}(E) := \sum_{S_z} (\rho^{NSS_z}(E))_{L_z L_z'}$. For example, since there exists only one configuration for occupation $N = 6$, $\rho^6$ is a number. On the other hand, $\rho^5(E_{5_0})$ is the $2 \times 2$ matrix associated to the 5-particles groundstate. By using the Wigner-Eckart theorem [37] to calculate matrix elements of creation and annihilation operators, $d_{\alpha\sigma}^\dagger$ and $d_{\alpha\sigma}$, between states of different particle number and spin, and summing over $\sigma$, Eq. (2) yields for the case of unidirectional transport near the $5_0 \leftrightarrow 6$ resonance [35]

$$0 = -i \left[ \sum_\alpha \omega_\alpha \mathcal{R}_\alpha, \rho^5 \right] + 2\Gamma \mathcal{R}_R \rho^6 - \frac{\Gamma}{2} \{ \mathcal{R}_L, \rho^5 \}, \quad (6)$$

which, together with $\text{Tr}_{\text{TQD}}\{\rho\} = 1$, fully determines $\rho^6$ and $\rho^5(E_{5_0})$. The first term on the r.h.s. of Eq. (6) is the Lamb shift contribution. The remaining terms are fully characterized by the rate matrix $(\mathcal{R}_\alpha)_{mn} = \frac{1}{2} \sum_\sigma \langle 5, E_{5_0}; \frac{1}{2}, -\sigma, m | d_{\alpha\sigma} | 6 \rangle \langle 6 | d_{\alpha\sigma}^\dagger | 5, E_{5_0}; \frac{1}{2}, -\sigma, n \rangle$, with $m, n = \pm 1$. A transformation from the localized to the angular momentum basis, $d_{l\sigma}^\dagger = 1/\sqrt{3} \sum_\alpha e^{-i\alpha l 2\pi/3} d_{\alpha\sigma}^\dagger$, $(l = 0, \pm 1)$ readily yields $(\mathcal{R}_\alpha)_{mn} = \frac{1}{3} e^{i\alpha(n-m)2\pi/3}$. The matrices $\mathcal{R}_L$ and $\mathcal{R}_R$ cannot be diagonalized simultaneuously. In the basis spanned by the vectors $|c\rangle \propto |0\rangle - 2|1\rangle + |2\rangle$ and $|d\rangle \propto |0\rangle - |2\rangle$, with the latter decoupled from the left lead ($|j\rangle$ indicates a 5-particles state with a hole at site $j$), we get

$$\mathcal{R}_L = \frac{1}{3} \begin{pmatrix} 2 & 0 \\ 0 & 0 \end{pmatrix} \quad \text{and} \quad \mathcal{R}_R = \frac{1}{6} \begin{pmatrix} 1 & -i\sqrt{3} \\ i\sqrt{3} & 3 \end{pmatrix}. \quad (7)$$

Neglecting the Lamb shift term, the matrix $\rho^5(E_{5_0})$ is diagonal, with elements $\rho^{dd} = 1$, $\rho^{cc} = 0$ at deep interference blockade. The diagonal terms $2/3$, $0$ and $1/6$, $1/2$ of $\mathcal{R}_\alpha$ correspond to the weights $R_L^f$, $R_L^s$, and $R_R^f$, $R_R^s$, respectively. Using these values, Eq. (5) yields $F_{nv}^{IB} = 5/3$. Let us now turn at the impact of the Lamb shift term. It describes a precession of the Bloch vector $\mathbf{n}$ of the orbitally degenerate block $\rho^5(E_{5_0}) = p(I + \mathbf{n} \cdot \boldsymbol{\sigma})/2$, where $\boldsymbol{\sigma}$ is the vector of Pauli matrices, $p = \rho_{dd} + \rho_{cc}$, and the decoupled state points along the $z$-axis. The precession frequencies $\omega_\alpha$ account for virtual transitions
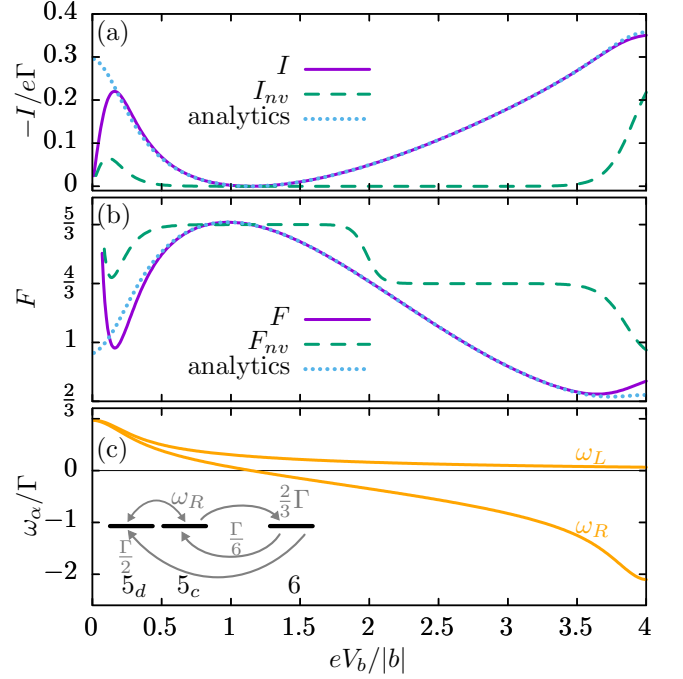


FIG. 3. Bias trace of (a) current, (b) Fano factor and (c) precession frequencies $\omega_{L,R}$ at $\xi = -7.5|b|$, corresponding to the green dashed line in Fig. 1. The numerical data well agree with analytical expressions from the text. Inset: the population of the coupled and decoupled states of the $5_0$ doublet depends on the effective rates for the $5_0 \leftrightarrow 6$ resonance and on the precession frequency $\omega_R$.

from the 5-particles groundstates to the state $|6\rangle$ and to levels with energies $E_{4_{0,1,2,3}}$, and are given in the Supplement. Their bias dependence is shown in Fig. 3(c). We find the stationary solution $\rho^{dd} = 1 - 3\omega_R^2/D$, $\rho_{cc} = 2\omega_R^2/D$ with $D = 2 + 8\omega_L^2 - 12\omega_L\omega_R + 9\omega_R^2$. Due to the precession, the populations of the decoupled and coupled states are affected by partially coherent gain and loss, as illustrated in the inset of Fig 3(c). The system gets quadratically stuck in the decoupled state for $\omega_R \to 0$. We find $I = -e4\Gamma\omega_R^2/3D$ and, to lowest order in $\omega_R$, $F = 5/3 + 16\omega_L\omega_R/3(1 + 4\omega_L^2)$ [35], yielding $\lim_{\omega_R \to 0} F = 5/3$. These formulas show good agreement with the numerics, as seen in Figs. 3(a) and 3(b). In the regime of linear conductance and Johnson-Nyquist noise the agreement is easily obtained by relieving unidirectionality [35].

*Conclusions.* – Using a full counting statistics approach in Liouville space we obtained the Fano stability diagram of a $C_{3v}$ symmetric TQD. In the region of current suppression the Fano factor helps unraveling the underlying blocking mechanisms. Poissonian statistics suggests "classical" Coulomb blockade, whereas super-Possonian noise (up to $F \gtrsim 6$) points to the presence of fast and slow channels. The value attained by the Fano factor at specific gate and bias voltages further re-

veals the internal level structure and dynamics of the system. In the case of interference blockade, we chose the $5_0 \leftrightarrow 6$ resonance to show that a population redistribution, induced by virtual excitations, results in a nontrivial bias dependence of the the Fano factor, which attains its maximal value $F = 5/3$ only when the blockade is perfect. Our results are robust against perturbations which weakly break the $C_{3v}$ symmetry, and hence orbital degeneracy, as long as the resulting level splitting is smaller than the coupling $\Gamma$ [38].

––––––––––––––

$^*$ E-mail: milena.grifoni@ur.de

[1] R. Landauer, Nature **392**, 658 (1998).

[2] S. Hershfield, J. H. Davies, P. Hyldgaard, C. J. Stanton, and J. W. Wilkins, Phys. Rev. B **47**, 1967 (1993).

[3] U. Hanke, Y. M. Galperin, K. A. Chao, and N. Zou, Phys. Rev. B **48**, 17209 (1993).

[4] A. N. Korotkov, Phys. Rev. B **49**, 10381 (1994).

[5] A. Nauen, I. Hapke-Wurst, F. Hohls, U. Zeitler, R. J. Haug, and K. Pierz, Phys. Rev. B **66**, 161303 (2002).

[6] D. A. Bagrets and Y. V. Nazarov, Phys. Rev. B **67**, 085316 (2003).

[7] A. Thielmann, M. H. Hettler, J. König, and G. Schön, Phys. Rev. B **68**, 115105 (2003).

[8] E. V. Sukhorukov, G. Burkard, and D. Loss, Phys. Rev. B **63**, 125315 (2001).

[9] A. Cottet and W. Belzig, Europhys. Lett. **66**, 405 (2004).

[4] W. Belzig, Phys. Rev. B **71**, 161301 (2005).

[11] G. Kießlich, A. Wacker, and E. Schöll, Phys. Rev. B **68**, 125320 (2003).

[12] C. W. Groth, B. Michaelis, and C. W. J. Beenakker, Phys. Rev. B **74**, 125315 (2006).

[13] C. Pöltl, C. Emary, and T. Brandes, Phys. Rev. B **80**, 115313 (2009).

[14] G. Schaller, G. Kießlich, and T. Brandes, Phys. Rev. B **80**, 245107 (2009).

[2] M. Korkusinski, I. P. Gimenez, P. Hawrylak, L. Gaudreau, S. A. Studenikin, and A. S. Sachrajda, Phys. Rev. B **75**, 115301 (2007).

[1] T. Kostyrko and B. R. Bułka, Phys. Rev. B **79**, 075310 (2009).

[5] A. Donarini, G. Begemann, and M. Grifoni, Nano Lett. **9**, 2897 (2009).

[18] H. Pan, M. G. House, X. Hao, and H. W. Jiang, Appl. Phys. Lett. **100**, 263109 (2012).

[19] M. Seo, H. K. Choi, S.-Y. Lee, N. Kim, Y. Chung, H.-S. Sim, V. Umansky, and D. Mahalu, Phys. Rev. Lett. **110**, 046803 (2013).

[20] S. Andergassen, Nature **495**, 321 (2013).

[21] S.-Y. Lee and Y. Chung, Phys. Rev. B **87**, 045302 (2013).

[22] M. Kotzian, F. Gallego-Marcos, G. Platero, and R. J. Haug, Phys. Rev. B **94**, 035442 (2016).

[23] L. Gaudreau, S. A. Studenikin, A. S. Sachrajda, P. Zawadzki, A. Kam, J. Lapointe, M. Korkusinski, and P. Hawrylak, Phys. Rev. Lett. **97**, 036807 (2006).

[24] H. H. Weitering, Nature Nanotech. **9**, 499 (2014).

[25] F. Domínguez, G. Platero, and S. Kohler, Chem. Phys. **375**, 284 (2010).

[26] I. Weymann, B. R. Bułka, and J. Barnaś, Phys. Rev. B **83**, 195302 (2011).

[27] K. Wrześniewski and I. Weymann, Phys. Rev. B **92**, 045407 (2015).

[28] A. Donarini, G. Begemann, and M. Grifoni, Phys. Rev. B **82**, 125451 (2010).

[3] C.-Y. Hsieh, Y.-P. Shim, M. Korkusinski, and P. Hawrylak, Rep. Prog. Phys. **75**, 114501 (2012).

[30] C. Flindt, T. Novotný, A. Braggio, and A.-P. Jauho, Phys. Rev. B **82**, 155407 (2010).

[31] F. Kaiser and S. Kohler, Annalen der Physik **16**, 702 (2007).

[32] M. G. Schultz and F. von Oppen, Phys. Rev. B **80**, 033302 (2009).

[33] F. Bodoky, W. Belzig, and C. Bruder, Phys. Rev. B **77**, 035302 (2008).

[34] W. Belzig and A. Bednorz, Phys. Status Solidi B **251**, 1945 (2014).

[35] Further information can be found in the Supplementary material.

[36] J. König, J. Schmid, H. Schoeller, and G. Schön, Phys. Rev. B **54**, 16820 (1996).

[37] A. Messiah, *Quantum Mechanics - Volume 2* (North Holland Physics Publishing, 1961).

[38] D. Darau, G. Begemann, A. Donarini, and M. Grifoni, Phys. Rev. B **79**, 235404 (2009).

SUPPLEMENTARY MATERIAL

**Many-body spectrum and eigenfunctions of a symmetric TQD**

The single particle part of the triple quantum dot Hamiltonian Eq. (1) is diagonalized in the basis of the angular momentum states $\{|l\rangle = 1/\sqrt{3}\sum_{\alpha=0}^{2} e^{-i\alpha l 2\pi/3}|\alpha\rangle,\ l = 0, \pm 1\}$. Accounting for the spin degree of freedom $\sigma$, we use this single particle basis to construct many-body states in the occupation number representation, where a generic vector $|n_{0\uparrow}, n_{1\uparrow}, n_{-1\uparrow}; n_{0\downarrow}, n_{1\downarrow}, n_{-1\downarrow}\rangle$ is fully characterized by the occupation numbers $n_{l\sigma}$. Finally, we use this many-body basis to diagonalize the TQD Hamiltonian $H_{\text{TQD}}$ and find its eigenvalues and eigenfunctions. $H_{\text{TQD}}$ commutes with the total particle number operator $N = \sum_{l\sigma} n_{l\sigma}$, the total spin operator $S^2 = \sum_{i\,l\sigma\sigma'}(d_{l\sigma}^\dagger s_{\sigma\sigma'}^i d_{l\sigma'})^2$ (here is $s^i = \frac{\hbar}{2}\sigma^i$ and $\sigma^i$ the $i$-th Pauli matrix), the spin projection $S_z = \frac{\hbar}{2}\sum_{l\sigma}\sigma n_{l\sigma}$, and the angular momentum operator $L_z = \hbar\sum_{l\sigma} l n_{l\sigma}|_{mod\,3}$. Hence, one can use the quantum numbers $N, S, S_z$ and $L_z$ associated to these operators together with the energy $E$ to characterize the eigenvectors of the interacting TQD Hamiltonian. In the following we use the notation $|N, E; S, S_z, L_z\rangle$ for a generic eigenvector. In particular, $S^2|N, E; S, S_z, L_z\rangle = \frac{\hbar}{2}S(S+1)|N, E; S, S_z, L_z\rangle$ and, as usual, $-S \leq S_z \leq S$. Such eigenvectors and the associated eigenvalues in the occupation number basis are reported in Tables I, II.

We notice that a classification of many-body states using the angular momentum quantum number $L_z$ has been proposed in [1] for the case of a symmetric triangular dot with intrasite repulsion only (i.e. $U \neq 0$, $V = 0$). Our analysis with $U \neq 0$, $V \neq 0$ thus generalizes that work and recovers the results reported in [2], where a localized representation is used to discuss topological Hund rules and derive effective low energy spin Hamiltonians. For finite onsite and intersite interactions $U$ and $V$, the composition of the eigenstates is the result of a complex interplay between Pauli statistics and Coulomb repulsion, and we refer to the review by [3] for useful insights. For example, for double occupancy of the TQD, the configurations with $S = 1$ corresponds to excited states with singly occupied dots, due to Pauli principle. The configurations with $S = 0$, however, contain both doubly occupied and singly occupied dots, with weight determined by the difference $U - V$. For $U = V$, the groundstate is in the occupation number representation the singlet $|100, 100\rangle$, with equal weights on single and doubly occupied sites, as seen in Table I. The splitting between the sextuplet of excited states and the groundstate singlet is dominated by the hopping energy with a correction given by super-exchange processes due to the doubly occupied singlet configurations [2]. For a TQD with occupancy $N = 4$ (i.e. with two-holes), the groundstate is always a triplet if $b < 0$, as in our work. Finally, of relevance for the discussion in the main manuscript, the 5-particles groundstate is a quadruplet due to orbital and spin degeneracy while the first excited state is only spin degenerate.

**Current and Fano factor for a minimal model with one slow and one fast channel**

Let us consider a minimal system consisting of a single slow and fast channel which for example can be a groundstate in Coulomb blockade (CB) plus an excited state in the bias window, or the coupled and decoupled states in the case of interference blockade (IB) near the $5_0 \leftrightarrow 6$ resonance, as depicted in Figs. 1(b),(c) respectively, of the main manuscript. This system spends most of the time in the state corresponding to the slow channel and therefore the exponentially suppressed current is dominated by the bottleneck process of escaping this state. The Liouvillian $\mathcal{L}$ or the tunneling Liouvillian $\mathcal{L}_t$ are super-operators whose matrix elements are obtained from their action on the reduced density matrix. In order to obtain a suitable representation of such Liouvillians, it is convenient to work in the Liouville space, where the density matrix elements are ordered in a vector. Let us consider a situation of positive electrochemical potential, such that particle transport occurs from the left, $L$, to the right, $R$, lead. Then, far from resonance (e.g. inside the Coulomb blockade or interference blockade regions), we can approximate the Fermi functions to 1 or 0, except for the dominant slow process $\Gamma_R^s f_R^\pm$ which transfers an electron from the slow state $|s\rangle$ to a state $|p\rangle$ with one electron more ($p = +$) or less ($p = -$). Then, depending on whether $p = \pm$, the minimal Liouvillian for such a system with slow and fast $|f\rangle$ channels takes in the basis $\{|p\rangle\langle p|, |s\rangle\langle s|, |f\rangle\langle f|\}$ the form

$$\mathcal{L}_t^{CB} = \begin{pmatrix} -\Gamma_L^f - \Gamma_L^s - \Gamma_R^s & \Gamma_R^s f_R^- & \Gamma_R^f \\ \Gamma_L^s + \Gamma_R^s & -\Gamma_R^s f_R^- & 0 \\ \Gamma_L^f & 0 & -\Gamma_R^f \end{pmatrix}, \ p = - \qquad \mathcal{L}_t^{IB} = \begin{pmatrix} -\Gamma_R^f - \Gamma_R^s & \Gamma_R^s f_R^+ & \Gamma_L^f \\ \Gamma_R^s & -\Gamma_R^s f_R^+ & 0 \\ \Gamma_R^f & 0 & -\Gamma_L^f \end{pmatrix}, \ p = + \qquad (1)$$

for the two situations pictured in Fig. 1(b),(c). The corresponding current superoperators for the right lead are

$$
\mathcal{J}_{CB}^+ = \begin{pmatrix} 0 & \Gamma_R^s f_R^- & \Gamma_R^f \\ 0 & 0 & 0 \\ 0 & 0 & 0 \end{pmatrix}, \quad
\mathcal{J}_{CB}^- = \begin{pmatrix} 0 & 0 & 0 \\ \Gamma_R^s & 0 & 0 \\ 0 & 0 & 0 \end{pmatrix}, \quad
\mathcal{J}_{IB}^+ = \begin{pmatrix} 0 & 0 & 0 \\ \Gamma_R^s & 0 & 0 \\ \Gamma_R^f & 0 & 0 \end{pmatrix}, \quad
\mathcal{J}_{IB}^- = \begin{pmatrix} 0 & \Gamma_R^s f_R^+ & 0 \\ 0 & 0 & 0 \\ 0 & 0 & 0 \end{pmatrix}. \tag{2}
$$

In our considerations, $\Gamma_R^s f_R^\mp$ gives the bottleneck for transport in the CB and IB cases, respectively. To lowest order in $f_R^\pm$ this results in the current

$$
I_{CB} = -e \frac{\Gamma_R^s (\Gamma_L^f + \Gamma_L^s)}{\Gamma_L^s + \Gamma_R^s} f_R^-, \quad I_{IB} = -e \Gamma_R^f f_R^+. \tag{3}
$$

For high asymmetry between the couplings to the leads, $\Gamma_L^s \gg \Gamma_R^s$, Eq. (3) simplifies to $I_{CB} = -e \Gamma_R^s f_R^- (1 + \Gamma_L^f / \Gamma_L^s)$, in agreement with the finding in [4]. For a completely symmetric setup ($\Gamma_L^s = \Gamma_R^s = \Gamma^s$) the current in situation (b) is $I_{CB} = -e(\Gamma^f + \Gamma^s) f_R^- / 2$.

Similar calculations as for the current yield the Fano factors

$$
F_{nv}^{CB} = 1 + \frac{2\Gamma_L^f}{\Gamma_L^s + \Gamma_R^s}, \quad F_{nv}^{IB} = 1 + 2 \frac{\Gamma_R^f}{\Gamma_R^s}. \tag{4}
$$

The expression for case (b) simplifies to $F_{nv}^{CB} = 1 + 2\Gamma_L^f / \Gamma_L^s$ for high asymmetry [4], and to $F_{nv}^{CB} = 1 + \Gamma_L^f / \Gamma_L^s$ for the symmetric case. In all cases it holds $F > 1$.

### Current and Fano factor for a minimal model at $\xi = -7.5|b|$

A striking feature at the left side of the stability diagram, a Fano factor of $F = 4/3$, cannot be obtained considering a minimal model using only the 5- and 6-particle states. It appears at bias and gate voltages where $f_R^-(E_{5_0} - E_{4_0})$ overcomes $f_R^+(E_6 - E_{5_0})$ and the transition to the triplet of ground states with 4 particles becomes the new bottleneck of transport. At $\xi = -7.5|b|$, this happens at $eV_b = (E_6 - E_{4_0}) = V$. A minimal model can be written in the basis $\{|6\rangle\langle 6|, |d\rangle\langle d|, |c\rangle\langle c|, |4\rangle\langle 4|\}$, with the coupled $|c\rangle$, decoupled $|d\rangle$ and the channel $|4\rangle$ associated to the triplet $\{4, E_{4_0}; 1, S_z, 0\rangle\}$. The Liouvillian and current superoperators are

$$
\mathcal{L} = \begin{pmatrix}
-\Gamma_{R,65}^c - \Gamma_{R,65}^d & 0 & \Gamma_{L,65}^c & 0 \\
\Gamma_{R,65}^d & -\Gamma_{R,54}^d f_R^- & 0 & \Gamma_{L,54}^d + \Gamma_{R,54}^d \\
\Gamma_{R,65}^c & 0 & -\Gamma_{L,65}^c & \Gamma_{L,54}^c + \Gamma_{R,54}^c \\
0 & \Gamma_{R,54}^d f_R^- & 0 & -\Gamma_{L,54}^d - \Gamma_{R,54}^d - \Gamma_{L,54}^c - \Gamma_{R,54}^c
\end{pmatrix},
$$

$$
\mathcal{J}^+ = \begin{pmatrix}
0 & 0 & 0 & 0 \\
\Gamma_{R,65}^d & 0 & 0 & 0 \\
\Gamma_{R,65}^c & 0 & 0 & 0 \\
0 & \Gamma_{R,54}^d f_R^- & 0 & 0
\end{pmatrix}, \quad
\mathcal{J}^- = \begin{pmatrix}
0 & 0 & 0 & 0 \\
0 & 0 & 0 & \Gamma_{R,54}^d \\
0 & 0 & 0 & \Gamma_{R,54}^c \\
0 & 0 & 0 & 0
\end{pmatrix}, \tag{5}
$$

where $f_R^-$ is the Fermi function between the 5- and 4-particle groundstates at the right lead and is responsible for the bottleneck process. To lowest order in this Fermi function, the current and Fano factor read

$$
I = -e \Gamma_{R,54}^d f_R^- \frac{\Gamma_{L,54}^c (\Gamma_{R,65}^c + 2\Gamma_{R,65}^d) + \Gamma_{R,54}^c (\Gamma_{R,65}^c + \Gamma_{R,65}^d) + \Gamma_{L,54}^d \Gamma_{R,65}^d}{\Gamma_{R,65}^d (\Gamma_{L,54}^c + \Gamma_{R,54}^c + \Gamma_{L,54}^d + \Gamma_{R,54}^d)},
$$

$$
F = \frac{\Gamma_{L,54}^c \left(2(\Gamma_{R,65}^c)^2 + 5\Gamma_{R,65}^c \Gamma_{R,65}^d + 4(\Gamma_{R,65}^d)^2\right) + \Gamma_{R,54}^c \left(2(\Gamma_{R,65}^c)^2 + 3\Gamma_{R,65}^c \Gamma_{R,65}^d + (\Gamma_{R,65}^d)^2\right) + \Gamma_{L,54}^d (\Gamma_{R,65}^d)^2}{\Gamma_{R,65}^d (\Gamma_{L,54}^c (\Gamma_{R,65}^c + 2\Gamma_{R,65}^d) + \Gamma_{R,54}^c (\Gamma_{R,65}^c + \Gamma_{R,65}^d) + \Gamma_{L,54}^d \Gamma_{R,65}^d)}. \tag{6}
$$

The rate matrix for the $5_0 \leftrightarrow 4_0$ transition reads $(\mathcal{R}_\alpha)_{mn}^{5_0 \leftrightarrow 4_0} = \frac{1}{2} \sum_{\sigma,\tau} \langle 5, E_{5_0}; \frac{1}{2}, \sigma, m | d_{\alpha\tau}^\dagger \mathcal{P}_{4,E_{4_0}} d_{\alpha\tau} | 5, E_{5_0}; \frac{1}{2}, \sigma, n \rangle$, in the angular momentum basis, with $m, n = \pm 1$ and where $\mathcal{P}_{NE} = \sum_{S_z, L_z} |N, E; S, S_z, L_z\rangle\langle N, E; S, S_z, L_z|$ is the projector on the $N$-particle level with energy $E$ and spin $S$. Under the bias and gate voltage conditions considered here, the system still remains in the interference ground state blocking associated to the $5_0 \leftrightarrow 6$ transition. The

corresponding coupled-decoupled basis introduced shortly above Eq. (7) of the main text is thus the most convenient representation. With the help of the eigenstates listed in Table II and the Wigner-Eckart theorem one calculates, $\Gamma^d_{\alpha,54} = \frac{3}{2}\Gamma R^f_\alpha$ and $\Gamma^c_{\alpha,54} = \frac{3}{2}\Gamma R^s_\alpha$ with $R^{f/s}_\alpha$ as given below Eq.(7) in the main text. Finally, by substitution into Eq.(6), one obtains $I = -e\Gamma f^-_R/4$ and $F = 4/3$.

### Liouvillian, current and Fano factor at the $5_0 \leftrightarrow 6$ resonance

The far left part of the stability diagram shown in Fig. 2 is dominated by $5 \leftrightarrow 6$ particle transitions. As seen in Table II, there exists only one configuration with 6 electrons given by the state $|6\rangle := |6, E_6; 0, 0, 0\rangle$. On the other hand, when 5 electrons populate the TQD a total of 6 configurations are possible. In particular, for $b < 0$ the groundstate is the quadruplet $\{|5, E_{5_0}; 1/2, \pm 1/2, \pm 1\rangle\}$, due to both orbital and spin degeneracy. The first excited state is the doublet $\{|5, E_{5_1}; 1/2, \pm 1/2, 0\rangle\}$ and is only spin degenerate. In this section we provide the explicit form of the tunneling Liouvillian $\mathcal{L}_t$ when the Fock space is restricted to the subspaces associated to the 5- and 6-particles groundstates. Such a Liouvillian determines the stationary reduced density matrices $\rho^5(E_{5_0})$ and $\rho^6$ when Lamb shifts are neglected. Since the 6 particle groundstate is a singlet, $\rho^6$ is just a $1 \times 1$ matrix. On the other hand, the calculation of $\rho^5(E_{5_0})$ involves first the evaluation of the matrix elements $\rho^{5\frac{1}{2}S_z}_{L_z L'_z} = \langle 5, E_{5_0}; 1/2, S_z, L_z | \rho^\infty | 5, E_{5_0}; 1/2, S_z, L'_z\rangle$, and then a summation over $S_z$: $\rho^5_{L_z L'_z} := \sum_{S_z} \rho^{5\frac{1}{2}S_z}_{L_z L_z}$. Hence, $\rho^5(E_{5_0})$ is a $2 \times 2$ matrix in a basis spanned by the vectors $|5^+_0\rangle$ and $|5^-_0\rangle$, where $\pm$ refers to the associated values of the angular momentum. Notice that coherences between states with the same particle number but different angular momentum have to be considered. We choose the basis $\{|5^+_0\rangle\langle 5^+_0|, |5^-_0\rangle\langle 5^-_0|, |6\rangle\langle 6|, |5^+_0\rangle\langle 5^-_0|, |5^-_0\rangle\langle 5^+_0|\}$. Then the tunneling Liouvillian can be written as

$$\mathcal{L}_t = \frac{\Gamma}{3} \begin{pmatrix} -f^+_R - f^+_L & 0 & 2(f^-_R + f^-_L) & \frac{1}{2}X & \frac{1}{2}X^* \\ 0 & -f^+_R - f^+_L & 2(f^-_R + f^-_L) & \frac{1}{2}X & \frac{1}{2}X^* \\ f^+_R + f^+_L & f^+_R + f^+_L & -4(f^-_R + f^-_L) & -X & -X^* \\ \frac{1}{2}X^* & \frac{1}{2}X^* & 2(1 + X^*) & -f^+_R - f^+_L & 0 \\ \frac{1}{2}X & \frac{1}{2}X & 2(1 + X) & 0 & -f^+_R - f^+_L \end{pmatrix}, \tag{7}$$

with the short notation $X = e^{-i\frac{2\pi}{3}} f^+_R + e^{i\frac{2\pi}{3}} f^+_L$. Note that the phases $e^{\pm i\frac{2\pi}{3}}$ arise from changing from position into angular momentum basis. The solution of the equation $\mathcal{L}_t \rho^\infty = 0$, together with the constraint $\text{Tr}_{\text{TQD}}\{\rho^\infty\} = 1$ (with $\text{Tr}_{\text{TQD}} = (1, 1, 1, 0, 0)$), yields the stationary density matrix vector

$$\rho^\infty = \frac{1}{2(f^+_R f^-_L + f^+_L f^-_R) + f^+_R f^+_L} \begin{pmatrix} f^+_R f^-_L + f^+_L f^-_R \\ f^+_R f^-_L + f^+_L f^-_R \\ f^+_R f^+_L \\ \frac{1}{2}(f^+_R - f^+_L)\left[\frac{f^+_R - f^+_L}{f^+_R + f^+_L} - i\sqrt{3}\right] \\ -\frac{1}{2}(f^+_R - f^+_L)\left[\frac{f^+_R - f^+_L}{f^+_R + f^+_L} + i\sqrt{3}\right] \end{pmatrix}. \tag{8}$$

The current operators for the right lead can be calculated along the same lines and read in the same basis

$$\mathcal{J}^+ = \frac{\Gamma}{3} f^-_R \begin{pmatrix} 0 & 0 & 2 & 0 & 0 \\ 0 & 0 & 2 & 0 & 0 \\ 0 & 0 & 0 & 0 & 0 \\ 0 & 0 & -2e^{i\frac{2\pi}{3}} & 0 & 0 \\ 0 & 0 & -2e^{-i\frac{2\pi}{3}} & 0 & 0 \end{pmatrix}, \quad \mathcal{J}^- = \frac{\Gamma}{3} f^+_R \begin{pmatrix} 0 & 0 & 0 & 0 & 0 \\ 0 & 0 & 0 & 0 & 0 \\ 1 & 1 & 0 & -e^{-i\frac{2\pi}{3}} & -e^{i\frac{2\pi}{3}} \\ 0 & 0 & 0 & 0 & 0 \\ 0 & 0 & 0 & 0 & 0 \end{pmatrix}, \tag{9}$$

which results in the current through the drain lead

$$I = -e\frac{\Gamma}{3} \frac{(f^+_L - f^+_R)f^+_R f^+_L}{(f^+_R + f^+_L)\left[2(f^+_R f^-_L + f^+_L f^-_R) + f^+_R f^+_L\right]}, \tag{10}$$

and the Fano factor

$$
\begin{aligned}
F_{nv} =& \frac{2(3f_L^- + 1)(f_R^+)^2 \left((f_L^+)^2 + 2f_L^+ f_L^- - 2f_L^- f_R^+\right)}{(f_L^+ + f_R^+)(f_L^+ f_R^- + f_L^+ + 2f_L^- f_R^+)^2} + \frac{5(f_L^+)^2 + 5f_L^+ f_R^+ + 3(f_R^+)^2}{(f_L^+ + f_R^+)^2} \\
&+ \frac{f_R^+ \left((f_L^+)^2(-(8f_L^- + f_R^+ + 4)) + 4f_L^+ f_L^- f_R^+ + 4f_L^- (f_R^+)^2\right)}{(f_L^+ + f_R^+)^2(f_L^+ f_R^- + f_L^+ + 2f_L^- f_R^+)} + \frac{6f_L^- f_R^+}{f_R^+ - f_L^+}
\end{aligned}
\tag{11}
$$

Away from resonance lines, the Fermi functions can be approximated by step functions. Setting $f_L^+ = f_R^- = 1$, $f_L^- = f_R^+ = 0$ (valid at positive electrochemical potential $eV_{\mathrm{b}}$), the Liouvillian simplifies to

$$
\mathcal{L}_t = \frac{\Gamma}{3}
\begin{pmatrix}
-1 & 0 & 2 & \frac{Y}{2} & \frac{Y^*}{2} \\
0 & -1 & 2 & \frac{Y}{2} & \frac{Y^*}{2} \\
1 & 1 & -4 & -Y & -Y^* \\
\frac{Y^*}{2} & \frac{Y^*}{2} & 2(1+Y^*) & -1 & 0 \\
\frac{Y}{2} & \frac{Y}{2} & 2(1+Y) & 0 & -1
\end{pmatrix},
\tag{12}
$$

where $Y = e^{i2\pi/3}$. Similarly, the density matrix becomes

$$
\rho^\infty = \left(\frac{1}{2}, \frac{1}{2}, 0, -\frac{i}{i+\sqrt{3}}, \frac{i}{-i+\sqrt{3}}\right)^\top,
\tag{13}
$$

which shows full occupation of the 5-particles groundstates and an empty 6-particles state. Therefore the current through the system is blocked. Since the $5_0$ groundstates block the current, one speaks of groundstates blockade [5]. The stability diagram for the current, Fig. 2(a) in the main manuscript, shows how the current gets strongly suppressed at the groundstates blockade and only features a small line of finite current at the groundstates resonance, $E_6(V_{\mathrm{g}}, V_{\mathrm{b}}) = E_{5_0}(V_{\mathrm{g}}, V_{\mathrm{b}})$.

As expected, the Fano factor is Poissonian, $F = 1$, in the region of the 6 particles Coulomb diamond and diverges for $V_{\mathrm{b}} \to 0$. In the region of the groundstates blockade it has the super-Poissonian value of $F_{nv} = 5/3$, in agreement with the full numerical results shown in Fig. 2(c).

## Interference dynamics

The Lamb shift Hamiltonian in Eq. (6) can be cast, following [5] into the form $H_{\mathrm{LS}} = \hbar \sum_\alpha \omega_\alpha \mathcal{R}_\alpha$ where the precession frequencies for the block $\rho^N(E^*)$ with spin $S$ is independent on $S_z$ ($\omega_{\alpha,S_z} = \omega_\alpha$)

$$
\begin{aligned}
\omega_{\alpha,S_z} =& \frac{\Gamma_\alpha}{2\pi} \sum_{S_z', E} \langle N, E^*; S, S_z, L_z | d_{0S_z'} \mathcal{P}_{N+1,E} d_{0S_z'}^\dagger | N, E^*; S, S_z, -L_z \rangle p_\alpha (E - E^*) \\
&+ \langle N, E^*; S, S_z, L_z | d_{0S_z'}^\dagger \mathcal{P}_{N-1,E} d_{0S_z'} | N, E^*; S, S_z, -L_z \rangle p_\alpha (E^* - E)
\end{aligned}
\tag{14}
$$

where $\mathcal{P}_{NE} = \sum_{S_z, L_z} |N, E; S, S_z, L_z\rangle \langle N, E; S, S_z, L_z|$ is the projector on the $N$-particle level with energy $E$ and spin $S$. We defined the function $p_\alpha(\Delta E) = -\operatorname{Re} \psi[1/2 + i(\Delta E - \mu_\alpha)/2\pi k_{\mathrm{B}} T]$ where $T$ is the temperature, $\psi$ the digamma function and $\mu_\alpha$ the chemical potential of lead $\alpha$. The stationary density matrix in the ordering $\rho^{cc}, \rho^{dd}, \rho^6, \rho^{cd}, \rho^{dc}$ obtained as solution to Eq. (6) is

$$
\rho^\infty = \frac{1}{2 + 8\omega_L^2 - 12\omega_L\omega_R + 9\omega_R^2}
\begin{pmatrix}
2\omega_R^2 \\
2 + 8\omega_L^2 - 12\omega_L\omega_R + 6\omega_R^2 \\
\omega_R^2 \\
2\sqrt{3}\omega_R(1 + i(\omega_L - \omega_R)) \\
2\sqrt{3}\omega_R(1 - i(\omega_L - \omega_R))
\end{pmatrix},
\tag{15}
$$

The corresponding current is

$$
I = -e\frac{\Gamma}{3}\frac{4\omega_R^2}{2 + 8\omega_L^2 - 12\omega_L\omega_R + 9\omega_R^2}.
\tag{16}
$$

For $\omega_R \to 0$ the system gets quadratically stuck in the decoupled state and thus current is supressed. The resulting Fano factor is

$$F = \frac{20 + 320\omega_L^4 - 704\omega_L^3\omega_R + 32\omega_R^2 + 195\omega_R^4 - 16\omega_L\omega_R(11 + 36\omega_R^2) + 16\omega_L^2(10 + 53\omega_R^2)}{3(2 + 8\omega_L^2 - 12\omega_L\omega_R + 9\omega_R^2)^2}, \tag{17}$$

which to lowest order in $\omega_R$ is $F = 5/3 + 16\omega_L\omega_R/3(1+4\omega_L^2)$. Therefore, the limit of $F = 5/3$ is recovered at complete blockade. Since $\omega_L > 0$, the Fano factor is not maximal at $\omega_R = 0$ but instead at a little lower bias voltage.

———————

* E-mail: milena.grifoni@ur.de
[1] T. Kostyrko and B. R. Bułka, Phys. Rev. B **79**, 075310 (2009).
[2] M. Korkusinski, I. P. Gimenez, P. Hawrylak, L. Gaudreau, S. A. Studenikin, and A. S. Sachrajda, Phys. Rev. B **75**, 115301 (2007).
[3] C.-Y. Hsieh, Y.-P. Shim, M. Korkusinski, and P. Hawrylak, Rep. Prog. Phys. **75**, 114501 (2012).
[4] W. Belzig, Phys. Rev. B **71**, 161301 (2005).
[5] A. Donarini, G. Begemann, and M. Grifoni, Nano Lett. **9**, 2897 (2009).

| $N$ | Eigenenergy | $S$ | $S_z$ | $L_z$ | Eigenstate in the basis $\{|n_{0\uparrow}, n_{1\uparrow}, n_{-1\uparrow}; n_{0\downarrow}, n_{1\downarrow}, n_{-1\downarrow}\rangle\}$ |
|---|---|---|---|---|---|
| 0 | $E_0 = 0$ | 0 | 0 | 0 | $|000,000\rangle$ |
| 1 | $E_{1_0} = \xi - \frac{U}{2} - 2V + 2b$ | $\frac{1}{2}$ | $-\frac{1}{2}$ | 0 | $|000,100\rangle$ |
| | | | $\frac{1}{2}$ | | $|100,000\rangle$ |
| | $E_{1_1} = \xi - \frac{U}{2} - 2V - b$ | $\frac{1}{2}$ | $-\frac{1}{2}$ | $-1$ | $|000,001\rangle$ |
| | | | | 1 | $|000,010\rangle$ |
| | | | $\frac{1}{2}$ | $-1$ | $|001,000\rangle$ |
| | | | | 1 | $|010,000\rangle$ |
| 2 | $E_{2_0} = 2\xi - U - 3V + b + \frac{U-V}{2} - s_2^-$ | 0 | 0 | 0 | $\cos(\phi_2)|100,100\rangle - \sin(\phi_2)\frac{1}{\sqrt{2}}(|010,001\rangle + |001,010\rangle)$ |
| | $E_{2_1} = 2\xi - U - 3V + b$ | 1 | $-1$ | $-1$ | $|000,101\rangle$ |
| | | | | 1 | $|000,110\rangle$ |
| | | | 0 | $-1$ | $\frac{1}{\sqrt{2}}(|100,001\rangle - |001,100\rangle)$ |
| | | | | 1 | $\frac{1}{\sqrt{2}}(|100,010\rangle - |010,100\rangle)$ |
| | | | 1 | $-1$ | $|101,000\rangle$ |
| | | | | 1 | $|110,000\rangle$ |
| | $E_{2_2} = 2\xi - U - 3V - \frac{b}{2} + \frac{U-V}{2} - s_1^+$ | 0 | 0 | $-1$ | $\cos(\phi_1)|010,010\rangle - \sin(\phi_1)\frac{1}{\sqrt{2}}(|100,001\rangle + |001,100\rangle)$ |
| | | | | 1 | $\cos(\phi_1)|001,001\rangle - \sin(\phi_1)\frac{1}{\sqrt{2}}(|100,010\rangle + |010,100\rangle)$ |
| | $E_{2_3} = 2\xi - U - 3V - 2b$ | 1 | $-1$ | 0 | $|000,011\rangle$ |
| | | | 0 | | $\frac{1}{\sqrt{2}}(|010,001\rangle - |001,010\rangle)$ |
| | | | 1 | | $|011,000\rangle$ |
| | $E_{2_4} = 2\xi - U - 3V - \frac{b}{2} + \frac{U-V}{2} + s_1^+$ | 0 | 0 | $-1$ | $\sin(\phi_1)|010,010\rangle + \cos(\phi_1)\frac{1}{\sqrt{2}}(|100,001\rangle + |001,100\rangle)$ |
| | | | | 1 | $\sin(\phi_1)|001,001\rangle + \cos(\phi_1)\frac{1}{\sqrt{2}}(|100,010\rangle + |010,100\rangle)$ |
| | $E_{2_5} = 2\xi + b - U - 3V + \frac{U-V}{2} + s_2^-$ | 0 | 0 | 0 | $\sin(\phi_2)|100,100\rangle + \cos(\phi_2)\frac{1}{\sqrt{2}}(|010,001\rangle + |001,010\rangle)$ |
| 3 | $E_{3_0} = 3\xi - \frac{3}{2}U - 3V + \frac{2}{3}(U-V)[1-\lambda_0/(2|a|)]$ | $\frac{1}{2}$ | $-\frac{1}{2}$ | $-1$ | $v_{0,1}|100,101\rangle - v_{0,2}|010,110\rangle - v_{0,3}|001,011\rangle$ |
| | | | | 1 | $v_{0,1}|100,110\rangle + v_{0,2}|001,101\rangle - v_{0,3}|010,011\rangle$ |
| | | | $-\frac{1}{2}$ | $-1$ | $v_{0,1}|101,100\rangle - v_{0,2}|110,010\rangle - v_{0,3}|011,001\rangle$ |
| | | | | 1 | $v_{0,1}|110,100\rangle - v_{0,2}|101,001\rangle + v_{0,3}|011,010\rangle$ |
| | $E_{3_1} = 3\xi - \frac{3}{2}U - 3V$ | $\frac{3}{2}$ | $-\frac{3}{2}$ | 0 | $|000,111\rangle$ |
| | | | $-\frac{1}{2}$ | | $\frac{1}{\sqrt{3}}(|001,110\rangle - |010,101\rangle + |100,011\rangle)$ |
| | | | $\frac{1}{2}$ | | $\frac{1}{\sqrt{3}}(|011,100\rangle - |101,010\rangle + |110,001\rangle)$ |
| | | | $\frac{3}{2}$ | | $|111,000\rangle$ |
| | $E_{3_2} = 3\xi - \frac{3}{2}U - 3V + \frac{2}{3}(U-V)[1-\lambda_1/(2|a|)]$ | $\frac{1}{2}$ | $-\frac{1}{2}$ | $-1$ | $v_{1,1}|110,100\rangle - v_{1,2}|101,001\rangle + v_{1,3}|011,010\rangle$ |
| | | | | 1 | $v_{1,1}|100,110\rangle + v_{1,2}|001,101\rangle - v_{1,3}|010,011\rangle$ |
| | | | $-\frac{1}{2}$ | v | $v_{1,1}|101,100\rangle - v_{1,2}|110,010\rangle - v_{1,3}|011,001\rangle$ |
| | | | | 1 | $v_{1,1}|100,101\rangle - v_{1,2}|010,110\rangle - v_{1,3}|001,011\rangle$ |
| | $E_{3_3} = 3\xi - \frac{3}{2}U - 3V + (U-V)$ | $\frac{1}{2}$ | $-\frac{1}{2}$ | 0 | $\frac{1}{\sqrt{2}}(|001,110\rangle - |100,011\rangle)$ |
| | | | | | $\frac{1}{\sqrt{6}}(|001,110\rangle + 2|010,101\rangle + |100,011\rangle)$ |
| | | | $\frac{1}{2}$ | | $\frac{1}{\sqrt{6}}(|110,001\rangle + 2|101,010\rangle + |011,100\rangle)$ |
| | | | | | $\frac{1}{\sqrt{2}}(|110,001\rangle - |011,100\rangle)$ |
| | $E_{3_4} = 3\xi - \frac{3}{2}U - 3V + \frac{2}{3}(U-V)[1-\lambda_{-1}/(2|a|)]$ | $\frac{1}{2}$ | $-\frac{1}{2}$ | $-1$ | $v_{-1,1}|100,101\rangle - v_{-1,2}|010,110\rangle - v_{-1,3}|001,011\rangle$ |
| | | | | 1 | $v_{-1,1}|100,110\rangle + v_{-1,2}|001,101\rangle - v_{-1,3}|010,011\rangle$ |
| | | | $\frac{1}{2}$ | $-1$ | $v_{-1,1}|101,100\rangle - v_{-1,2}|110,010\rangle - v_{-1,3}|011,001\rangle$ |
| | | | | 1 | $v_{-1,1}|110,100\rangle - v_{-1,2}|101,001\rangle + v_{-1,3}|011,010\rangle$ |

TABLE I. Eigenvalues and eigenstates of a $C_{3v}$ symmetric TQD Hamiltonian for occupation numbers $N = 0 - 3$. Such eigenvectors are furthermore characterized by the spin quantum numbers $S$ and $S_z$, and by the orbital quantum number $L_z$. Their composition in the basis of the occupation number vectors is provided in the rightmost column. The ordering of the eigenergies depends on the TQD parameters $b, U$ and $V$. We chose $U = 5|b|$, $V = 2|b|$ and $b < 0$. We defined $a = (U-V)/(9b)$, $\theta = \arccos\left(((3a^2)/(1+3a^2))^{\frac{3}{2}}\right)/3$, $\lambda_\alpha = 2\sqrt{(1+a^2)/3}\cos\left(\theta + \alpha\frac{2\pi}{3}\right)$, $v_{\alpha,1} = (a-\lambda_\alpha)|a-\lambda_\alpha - 1|\text{sgn}(a-\lambda_\alpha+1)/\sqrt{3(a-\lambda_\alpha)^4+1}$, $v_{\alpha,2} = |(a-\lambda_\alpha)^2-1|/\sqrt{3(a-\lambda_\alpha)^4+1}$, $v_{\alpha,3} = (a-\lambda_\alpha)|a-\lambda_\alpha + 1|\text{sgn}(a-\lambda_\alpha-1)/\sqrt{3(a-\lambda_\alpha)^4+1}$, $s_1^\pm = \frac{1}{2}\sqrt{9b^2 \pm 2b(U-V) + (U-V)^2}$, $s_2^\pm = \sqrt{9b^2 \pm b(U-V) + \left(\frac{U-V}{2}\right)^2}$, $\phi_1 = \frac{1}{2}\arctan\left(\frac{2\sqrt{2}(U-V)}{U-V+9b}\right)$ and $\phi_2 = \frac{1}{2}\arctan\left(\frac{2\sqrt{2}(U-V)}{U-V-18b}\right)$.

| $N$ | Eigenenergy | $S$ | $S_z$ | $L_z$ | Eigenstate in the basis $\{|n_{0\uparrow}, n_{1\uparrow}, n_{-1\uparrow}; n_{0\downarrow}, n_{1\downarrow}, n_{-1\downarrow}\rangle\}$ |
|---|---|---|---|---|---|
| 4 | $E_{4_0} = 4\xi + 2b - U - 3V$ | 1 | $-1$ | 0 | $|100, 111\rangle$ |
| | | | 0 | | $\frac{1}{\sqrt{2}}(|101, 110\rangle - |110, 101\rangle)$ |
| | | | 1 | | $|111, 100\rangle$ |
| | $E_{4_1} = 4\xi - U - 3V + \frac{b}{2} + \frac{U-V}{2} - s_1^-$ | 0 | 0 | $-1$ | $\cos(\phi_3)|110, 110\rangle + \sin(\phi_3)\frac{1}{\sqrt{2}}(|011, 101\rangle + |101, 011\rangle)$ |
| | | | | 1 | $\cos(\phi_3)|101, 101\rangle - \sin(\phi_3)\frac{1}{\sqrt{2}}(|011, 110\rangle + |110, 011\rangle)$ |
| | $E_{4_2} = 4\xi - U - 3V - b + \frac{U-V}{2} - s_2^+$ | 0 | 0 | 0 | $\cos(\phi_4)|011, 011\rangle + \sin(\phi_4)\frac{1}{\sqrt{2}}(|101, 110\rangle + |110, 101\rangle)$ |
| | $E_{4_3} = 4\xi - U - 3V - b$ | 1 | $-1$ | $-1$ | $|001, 111\rangle$ |
| | | | | 1 | $|010, 111\rangle$ |
| | | | 0 | $-1$ | $\frac{1}{\sqrt{2}}(|011, 101\rangle - |101, 011\rangle)$ |
| | | | | 1 | $\frac{1}{\sqrt{2}}(|011, 110\rangle - |110, 011\rangle)$ |
| | | | 1 | $-1$ | $|111, 001\rangle$ |
| | | | | 1 | $|111, 010\rangle$ |
| | $E_{4_4} = 4\xi - U - 3V + \frac{b}{2} + \frac{U-V}{2} + s_1^-$ | 0 | 0 | $-1$ | $\sin(\phi_3)|110, 110\rangle - \cos(\phi_3)\frac{1}{\sqrt{2}}(|011, 101\rangle + |101, 011\rangle)$ |
| | | | | 1 | $\sin(\phi_3)|101, 101\rangle + \cos(\phi_3)\frac{1}{\sqrt{2}}(|011, 110\rangle + |110, 011\rangle)$ |
| | $E_{4_5} = 4\xi - U - 3V - b + \frac{U-V}{2} + s_2^+$ | 0 | 0 | 0 | $-\sin(\phi_4)|011, 011\rangle + \cos(\phi_4)\frac{1}{\sqrt{2}}(|101, 110\rangle + |110, 101\rangle)$ |
| 5 | $E_{5_0} = 5\xi - \frac{U}{2} - 2V + b$ | $\frac{1}{2}$ | $-\frac{1}{2}$ | $-1$ | $|101, 111\rangle$ |
| | | | | 1 | $|110, 111\rangle$ |
| | | | $\frac{1}{2}$ | $-1$ | $|111, 101\rangle$ |
| | | | | 1 | $|111, 110\rangle$ |
| | $E_{5_1} = 5\xi - \frac{U}{2} - 2V - 2b$ | $\frac{1}{2}$ | $-\frac{1}{2}$ | 0 | $|011, 111\rangle$ |
| | | | $\frac{1}{2}$ | | $|111, 011\rangle$ |
| 6 | $E_6 = 6\xi$ | 0 | 0 | 0 | $|111, 111\rangle$ |

TABLE II. Eigenvalues and eigenstates of a $C_{3v}$ symmetric TQD for electron numbers $N = 4$–6. The parameters and notations are chosen as in Table I. The ordering is for $U = 5|b|$, $V = 2|b|$ and $b < 0$. We defined $s_1^\pm = \frac{1}{2}\sqrt{9b^2 \pm 2b(U-V) + (U-V)^2}$, $s_2^\pm = \sqrt{9b^2 \pm b(U-V) + \left(\frac{U-V}{2}\right)^2}$, $\phi_3 = \frac{1}{2}\arctan\left(\frac{2\sqrt{2}(U-V)}{U-V-9b}\right)$ and $\phi_4 = \frac{1}{2}\arctan\left(\frac{2\sqrt{2}(U-V)}{U-V+18b}\right)$.